

Instantaneous polarization attributes based on an adaptive approximate covariance method

Mamadou Sanou Diallo¹, Michail Kulesh², Matthias Holschneider²,
Kristina Kurennaya², and Frank Scherbaum³

ABSTRACT

We introduce a method for computing instantaneous-polarization attributes from multicomponent signals. This is an improvement on the standard covariance method (SCM) because it does not depend on the window size used to compute the standard covariance matrix. We overcome the window-size problem by deriving an approximate analytical formula for the cross-energy matrix in which we automatically and adaptively determine the time window. The proposed method uses polarization analysis as applied to multicomponent seismic by waveform separation and filtering.

INTRODUCTION

Polarization properties of seismic arrivals can be estimated from multicomponent data. The polarization can be used to distinguish surface from body waves or, more generally, for wavefield decomposition (Flinn, 1965; Kanasewich, 1981; Jurkevics, 1988; Jackson et al., 1991). For example, polarization knowledge is often used to design filters for noise reduction and to separate elliptically and linearly polarized signals (Montalbetti and Kanasewich, 1970; Reading et al., 2001). From polarization properties, it is possible to relate shear-wave splitting to anisotropy and to design filters that improve the signal-to-noise ratio.

The polarization analysis based on the covariance matrix of a three-component (3-C) record $S_x(t)$, $S_y(t)$, and $S_z(t)$ is done by the eigenanalysis of the cross-energy matrix \mathbf{M} (Flinn, 1965; Montalbetti and Kanasewich, 1970; Esmersoy, 1984; Jurkevics, 1988):

$$\mathbf{M}(\xi) = \begin{bmatrix} I_{xx}(\xi) & J_{xy}(\xi) & J_{xz}(\xi) \\ J_{xy}(\xi) & I_{yy}(\xi) & J_{yz}(\xi) \\ J_{xz}(\xi) & J_{yz}(\xi) & I_{zz}(\xi) \end{bmatrix}, \quad (1)$$

where

$$I_{kk}(\xi) = \frac{1}{T} \int_{\xi-T/2}^{\xi+T/2} (S_k(\tau) - \mu_k(\xi))^2 d\tau,$$

$$J_{km}(\xi) = \frac{1}{T} \int_{\xi-T/2}^{\xi+T/2} (S_k(\tau) - \mu_k(\xi))(S_m(\tau) - \mu_m(\xi)) d\tau,$$

$$k, m = (x, y, z).$$

In the above equations, ξ is the center position of the time window T , around which the covariance matrix is computed, and $\mu_k(\xi)$ is the mean value of each signal component in the analysis window. Eigenanalysis performed on the matrix $\mathbf{M}(\xi)$ yields the principal component decomposition of the energy for the time window. Such a decomposition yields three eigenvalues $\lambda_i(\xi)$ and three corresponding eigenvectors $\mathbf{v}_i(\xi)$ that fully characterize the magnitude and direction of the principal components of the ellipsoid that approximates the particle motion in the time window.

One critical issue in the application of the covariance method is selecting the window size. Moreover, because the eigenvalues

Manuscript received by the Editor May 9, 2005; revised manuscript received January 9, 2006; published online August 28, 2006.

¹Formerly University of Potsdam, Germany; presently ExxonMobil Upstream Research Company, 3319 Mercer Street, Houston, Texas 77027. E-mail: mamadou.s.diallo@exxonmobil.com.

²University of Potsdam, Applied and Industrial Mathematics, Am Neuen Palais 10, 14469 Potsdam, Germany. E-mail: mkulesh@math.uni-potsdam.de; hols@math.uni-potsdam.de; kurinna@math.uni-potsdam.de.

³University of Potsdam, Faculty of Geoscience, Karl-Liebnicht-Strasse 24-25, 14414 Postdam, Germany. E-mail: fs@geo.uni-potsdam.de.

© 2006 Society of Exploration Geophysicists. All rights reserved.

(eigenvectors) are estimated once for each window, one needs an interpolation procedure to determine the parameters at each sample point prior to using them for filtering or denoising purposes. Vidale (1986) used the Hilbert transform of the multicomponent signal (component-wise) to construct the covariance matrix and determine subsequently the instantaneous ellipticity. Morozov and Smithson (1996) proposed another approach that allows an estimate of all the polarization parameters at each time and for any number of components but is limited to the case of an ellipse in 3D space. With this method, it is impossible to assess the strength of the polarization direction that is associated with the third eigenvalue obtained from equation 1.

For the case when seismic signals arrive simultaneously, it is sometimes difficult to select an optimal window unless the analysis is made in the time-frequency domain. Recently, Soma et al. (2002) made an extended-polarization analysis in the time-frequency domain (wavelet domain) with the help of continuous-wavelet transforms. This approach provides a better resolution of the polarization attributes but still requires that a time window be selected for the analysis.

In this paper, we introduce an approach that overcomes the constraint related to the window length. We achieve this by deriving an approximate analytical formula for the entries of the cross-energy matrix (equation 1) in which the time window T is adaptively selected. This approximation can be applied directly to wavefield separation and filtering of multicomponent seismic records using polarization analysis or can design methods based on cross-energy matrix calculation in the wavelet domain.

ADAPTIVE APPROXIMATE CROSS-ENERGY MATRIX METHOD

Let $S_k^H(t)$ be the Hilbert transform of the signal $S_k(t)$, $k = (x, y, z)$. Then $C_k(t) = S_k(t) + iS_k^H(t)$ are the corresponding analytic signals. Locally, around t , we can write

$$\begin{aligned} S_k(t + \tau) &\simeq \frac{1}{2}(C_k(t)e^{i\Omega_k(t)\tau} + C_k^*(t)e^{-i\Omega_k(t)\tau}) \\ &= |C_k(t)|\cos(\Omega_k(t)\tau + \arg C_k(t)), \end{aligned} \quad (2)$$

where $\Omega_k(t) = d/dt \arg C_k(t)$ are the instantaneous frequencies and $(\cdot)^*$ indicates the complex conjugate.

Using the approximations of equation 2 for each component $S_k(t)$, we can rewrite the cross-energy matrix as

$$\tilde{\mathbf{M}}(t) = \begin{bmatrix} \tilde{I}_{xx}(t) & \tilde{I}_{xy}(t) & \tilde{I}_{xz}(t) \\ \tilde{I}_{xy}(t) & \tilde{I}_{yy}(t) & \tilde{I}_{yz}(t) \\ \tilde{I}_{xz}(t) & \tilde{I}_{yz}(t) & \tilde{I}_{zz}(t) \end{bmatrix}, \quad (3)$$

where

$$\begin{aligned} \tilde{I}_{km}(t) &= \frac{1}{T_{km}(t)} \int_{-T_{km}(t)/2}^{T_{km}(t)/2} (S_k(t + \tau) - \mu_{km}) \\ &\quad \times (S_m(t + \tau) - \mu_{mk}) d\tau = |C_k(t)||C_m(t)| \\ &\quad \times \left\{ \text{sinc} \left[\frac{\Omega_k(t) - \Omega_m(t)}{2} T_{km}(t) \right] \right. \\ &\quad \times \cos[\arg C_k(t) - \arg C_m(t)] \\ &\quad \left. + \text{sinc} \left[\frac{\Omega_k(t) + \Omega_m(t)}{2} T_{km}(t) \right] \right. \\ &\quad \left. \times \cos[\arg C_k(t) + \arg C_m(t)] \right\} - \mu_{km}\mu_{mk}, \end{aligned}$$

and the mean value μ_{km} is defined as

$$\begin{aligned} \mu_{km} &= \frac{1}{T_{km}(t)} \int_{-T_{km}(t)/2}^{T_{km}(t)/2} S_k(t + \tau) d\tau \\ &= \Re[C_k(t)] \text{sinc}[T_{km}(t)\Omega_k(t)/2]. \end{aligned} \quad (4)$$

In the expression above, $\text{sinc}(x)$ represents the sine cardinal function and $\Re(\cdot)$ is the real part of a complex value. Note that unlike $\mathbf{M}(\xi)$, the matrix $\tilde{\mathbf{M}}(t)$ is defined for each time t , which is the main advantage over the standard covariance method (SCM).

Given the three eigenvalues $\lambda_1(t) \geq \lambda_2(t) \geq \lambda_3(t)$ and the corresponding eigenvectors $\mathbf{v}_k(t)$ obtained from the eigenanalysis of $\tilde{\mathbf{M}}(t)$, one can compute the usual instantaneous attributes for the polarization ellipsoid:

$$\begin{aligned} R_{\max}(t) &= \sqrt{\lambda_1(t)}, \quad R_{\text{med}}(t) = \sqrt{\lambda_2(t)}, \quad R_{\min}(t) = \sqrt{\lambda_3(t)}, \\ \mathbf{R}_{\max}(t) &= R_{\max}(t) \frac{\mathbf{v}_1(t)}{\|\mathbf{v}_1(t)\|}, \quad \mathbf{R}_{\text{med}}(t) = R_{\text{med}}(t) \frac{\mathbf{v}_2(t)}{\|\mathbf{v}_2(t)\|}, \\ \mathbf{R}_{\min}(t) &= R_{\min}(t) \frac{\mathbf{v}_3(t)}{\|\mathbf{v}_3(t)\|}, \end{aligned} \quad (5)$$

where $R_{\max}(t)$ is the instantaneous major axis, and $R_{\text{med}}(t)$ and $R_{\min}(t)$ are the two instantaneous minor axes. Bold characters indicate that the considered parameter is vectorial rather than scalar.

Here, $T_{km}(t)$ represents the adaptive time window used in equations 3 and 4. We propose two ways of determining this parameter. For example, one can choose $T_{km}(t)$ to be the same for all entries of the cross-energy matrix $\tilde{\mathbf{M}}(t)$ as

$$T_{km}(t) = \frac{6\pi N}{\Omega_x(t) + \Omega_y(t) + \Omega_z(t)} = \frac{2\pi N}{\Omega_{av}^{xyz}(t)}, \quad (6)$$

or define it in a specific manner for each entry as

$$T_{km}(t) = \frac{4\pi N}{\Omega_k(t) + \Omega_m(t)} = \frac{2\pi N}{\Omega_{av}^{km}(t)}. \quad (7)$$

From equation 2, we note that each signal is locally approximated by a cosine function with a period of $2\pi/\Omega_k(t)$. To elucidate the rationale behind the definition of the adaptive window $T_{km}(t)$ as given

in equations 6 and 7, we consider the situation where $\Omega_x(t) = \Omega_y(t) = \Omega_z(t) = \Omega(t)$. In this case, $T_{km}(t)$ from both equations 6 and 7 is reduced to $2\pi N/\Omega(t)$, which is an integer of the period. With N as an integer, we ensure that the integration in equations 3 and 4 is always performed over a window covering complete cycles of the signal.

In general, the instantaneous frequencies from the different components are different, and $T_{km}(t)$ as defined in equations 6 and 7 will still represent an average period. In such a situation, equation 7 provides a better estimate for the optimal adaptive-time window.

The effect of varying the parameter N is shown in Figure 1. Figure 1a shows three signals $S_x(t)$, $S_y(t)$, and $S_z(t)$ (black solid line) and their respective local approximations using equation 2 (gray solid line). For this example, we used slightly different instantaneous frequencies for $S_x(t)$, $S_y(t)$, and $S_z(t)$. The adaptive time window for these signals obtained from equation 6 with $N = 1$ is approximately 0.05 s. In Figure 1a, we observe that for up to 0.05 s on the time axis, the approximations fit very well to the actual signals. Also, from the signal curves and the hodograph plot in Figure 1b, we see that all signals in this time interval have undergone approximately one full cycle. Moreover, this hodograph plot indicates that with $N = 1$, the polarization analysis would not be able to characterize a structure more complex than an ellipse in 3D space. From the curves in Figure 1a, as N increases, the accuracy of the approximations decrease. With the decrease in accuracy, a curve that is more complex than an ellipse starts to build up from the hodograph (Figure 1b). Therefore, an improvement in our ability to characterize an eventual third polarization direction with larger N comes at the expense of accurate approximations of the signals.

Note that the adaptive time window, as we define it here, could be applied for the standard cross-energy matrix given by equation 1. This would allow us to determine the polarization attributes at each time without interpolation, but it still would be difficult to determine the attributes at either end of the time series. For seismic signals from controlled sources, this problem can be overcome easily because the signal of interest often arrives with some time delay and dies off well before the end of the time series. This is not the case for seismic signals from passive sources because all time windows can contain useful information; thus, the polarization attributes will be defined poorly at the beginning and end of the time series.

NUMERICAL EXAMPLES

Synthetic 3-C signal

To illustrate the performance of the proposed method, we compare the polarization attributes to

those obtained with other methods. The analysis is performed on a synthetic 3-C signal (not based on a physical model) containing arrivals with different types of polarization as shown in Figure 2. Wave-group A simulates a stationary ellipse; wave-group B simulates a rotating ellipse, and wave-group C is that of a linearly polar-

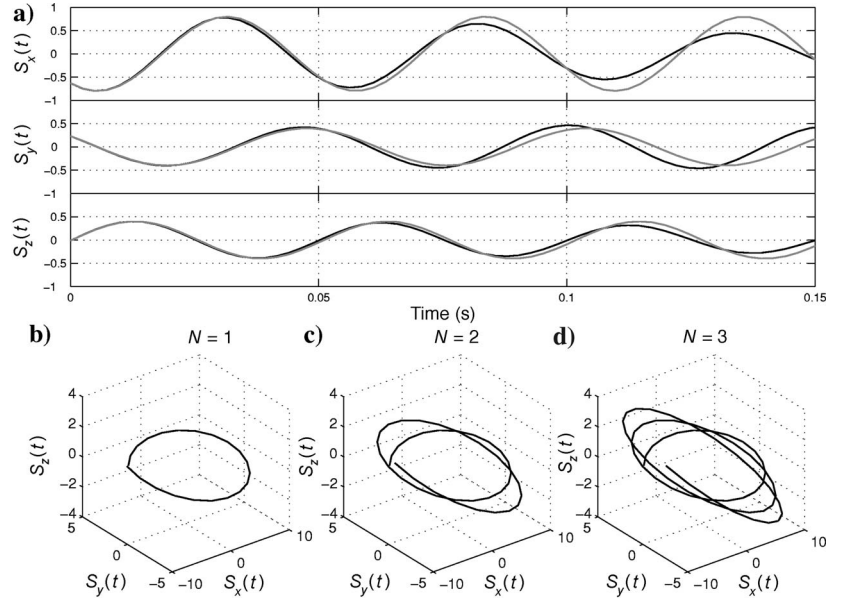


Figure 1. Illustration of the influence of increasing N in equations 4 and 5 on the accuracy of the approximation for the signals. (a) Three synthetic signals $S_x(t)$, $S_y(t)$, $S_z(t)$ (black solid lines) and the corresponding approximations (gray solid lines) for corresponding values of $N = 1, 2, 3$. (b, c, d) Hodograph plots for each segment of the approximated signals for the different values of N . For $N = 1$, the approximation is good up to 0.05 s, for $N = 2$ the approximation extends to 0.1 s and for $N = 3$ the approximation covers the entire time window of the synthetic signals. Note how the curves drift apart as N increases.

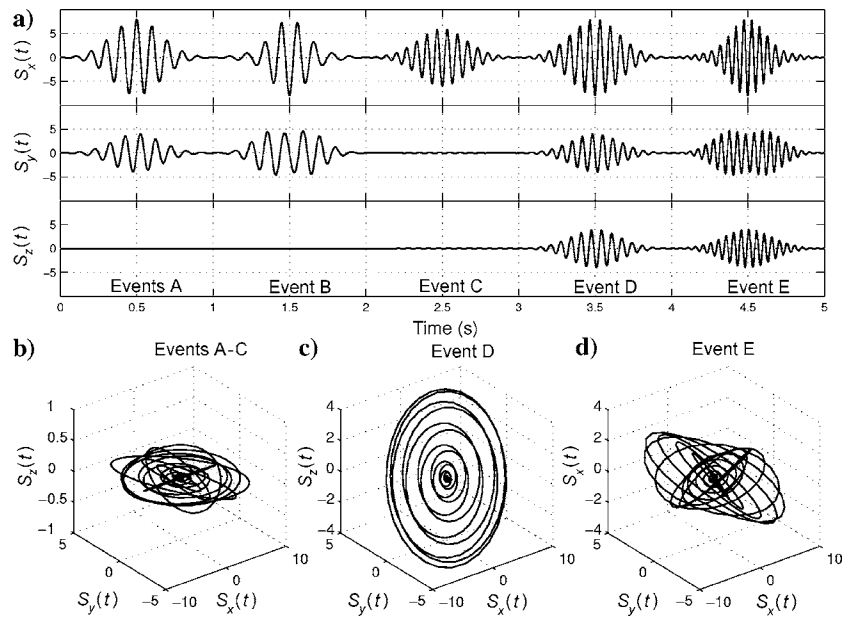


Figure 2. (a) Three synthetic signals simulating a 3-C record with elliptically polarized wave groups contained in the (x-z), (x-y), and (y-z) planes. Hodograph plots show the ellipses in the different polarization plane for wave groups (b) A–C, (c) for wave group D, and (d) for wave group E.

ized event. Wave-group D is a stationary ellipse in 3D space, and wave-group E corresponds to that of a rotating ellipsoid.

In Figure 3a, the major and minor axes of the polarization ellipse, computed from the proposed and Morozov's methods, are plotted as black curves next to those obtained from the standard covariance method (gray curves). Curves corresponding to the new method coincide with those of Morozov's method. Both methods give similar results for the major axis and the larger minor axis [$R_{\text{med}}(t)$] for all wave types. However, with the SCM, the determination of these axes is less accurate, as evidenced by the oscillating curves in Figure 3a. This is because of the constraint of finding the optimal time window as mentioned above.

For the ellipsoidal wave-group E, we note that aside from the oscillations observed for the curves from the SCM, all methods give similar results for the major and larger minor axes estimates. But only the SCM and the new method can provide an estimate for the third (smaller) polarization axis. However, the estimate of the third polarization is not unique and depends upon the selected window length for the SCM and by the value of the integer N in equation 7.

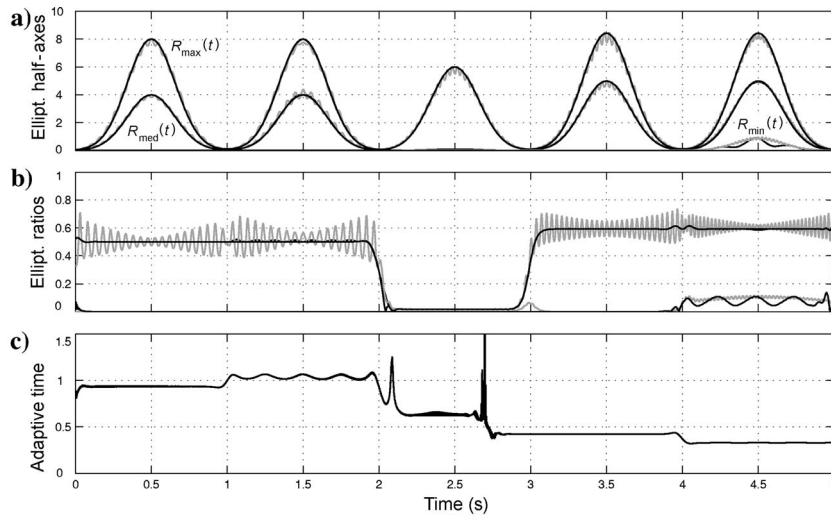


Figure 3. 3D instantaneous-polarization attributes in the time domain: (a) instantaneous major, minor, and second minor axes; (b) ellipticity ratio; (c) adaptive time window. From the ellipticity ratios, one can identify clearly the linearly polarized wave group [$R_{\text{med}}(t)/R_{\text{max}}(t)$ close to zero] from those with elliptical or ellipsoidal polarization.

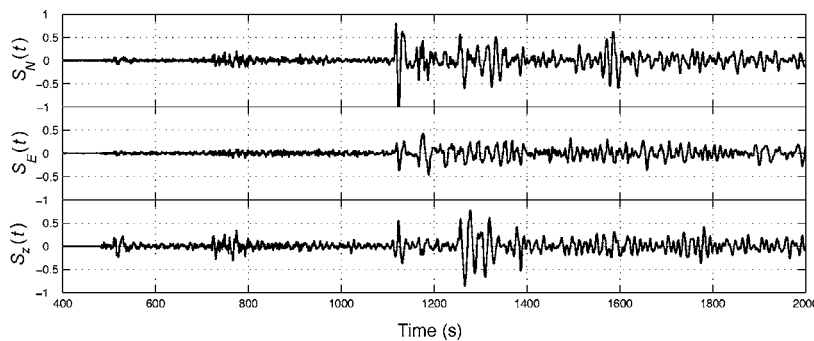


Figure 4. 3-C seismogram originating from the June 13, 2005 earthquake in the Chile-Bolivia border region recorded at the German Regional Seismic Network (GRSN) station. The magnitude was determined at $MW = 7.8$.

We show the ellipticity ratio in Figure 3b. For events A, B, C, and D, we plot the ratio $R_{\text{med}}(t)/R_{\text{max}}(t)$; for the last wave group we plot both $R_{\text{med}}(t)/R_{\text{max}}(t)$ and $R_{\text{min}}(t)/R_{\text{max}}(t)$. Consistent results are observed for all methods. With these parameters, one can distinguish clearly the linearly polarized wave groups from those with elliptical or ellipsoidal polarization. However, with the SCM, the estimated attributes show a high degree of variance.

Figure 3c shows the adaptive time window obtained using equation 6. As can be observed, the length of the adaptive window decreases as the frequency of the signal increases and vice versa.

Real 3-C record

We tested the adaptive-covariance method (ACM) on the real 3-C seismic record shown in Figure 4 and compared the result with the SCM. In Figure 5, we compare the major and minor axes of polarization computed from the ACM (black curves) and the SCM (gray curves). Here, again, the center of the time window for the SCM is shifted each time by one sample as in the synthetic example. As one

can see by comparing the black and gray curves, the standard method represents a smoothed version of the instantaneous attributes from the adaptive method. Furthermore, because the time window is fixed for the standard method, it is not possible to characterize polarization attributes of a seismic event with a period lower than that of the time window used for the analysis.

We circumvent this problem with the ACM through the adaptive selection of the time window. Note that the two curves agree quite well in the region where the period of the dominant signal is close to the time window selected for the covariance analysis. In general, regions where the two curves from the two methods differ significantly indicate that the selected window for the SCM is not optimal.

We compared the results of the covariance-based filter (Kanasewich, 1981) on a seismogram from a recent earthquake in South America (Figures 4 and 5). The filter signal is

$$S_k^f(t) = S_k(t) \cdot R(t) \cdot D_k(t), \quad k = (x, y, z), \quad (8)$$

where $R(t) = [1 - (\lambda_2(t)/\lambda_1(t))^q]^p$ is the rectilinearity and $D_k(t) = |v_{1k}(t)|^d$ is the directionality computed using the normalized eigenvector corresponding to the largest eigenvalue. The quantities p , q , and d are determined empirically (Kanasewich, 1981).

We present the filtering results in Figure 6, where the panels show the source signal for each component, and the corresponding filtered seismograms with the SCM for different window lengths and with the ACM for different N values. With both methods, the filtering is applied twice. In the second pass, the filter has a time window five times larger than the filter used in the first pass. From the seismograms filtered with the

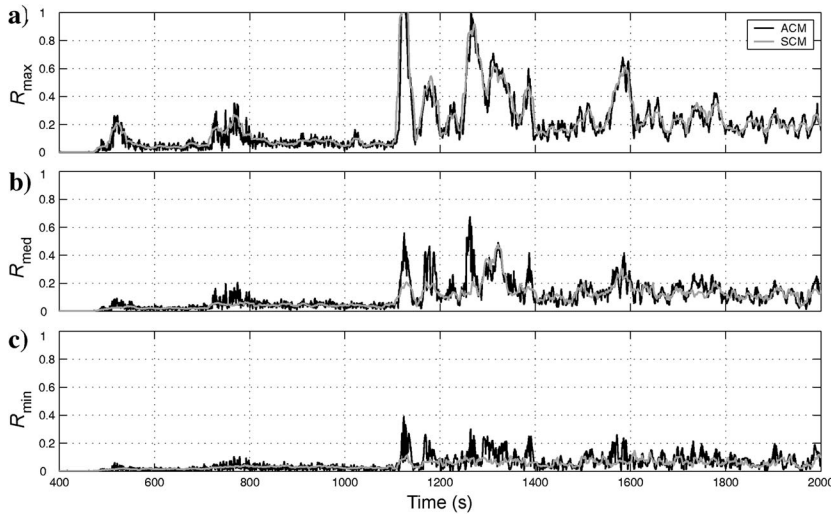


Figure 5. Comparison of the polarization attributes obtained from the ACM with those computed using SCM. (a) Major polarization axis, (b) second major polarization axis, (c) minor polarization axis. While the two methods agree well on the average trend of curves, our method shows more sensitivity to local variations of the attributes.

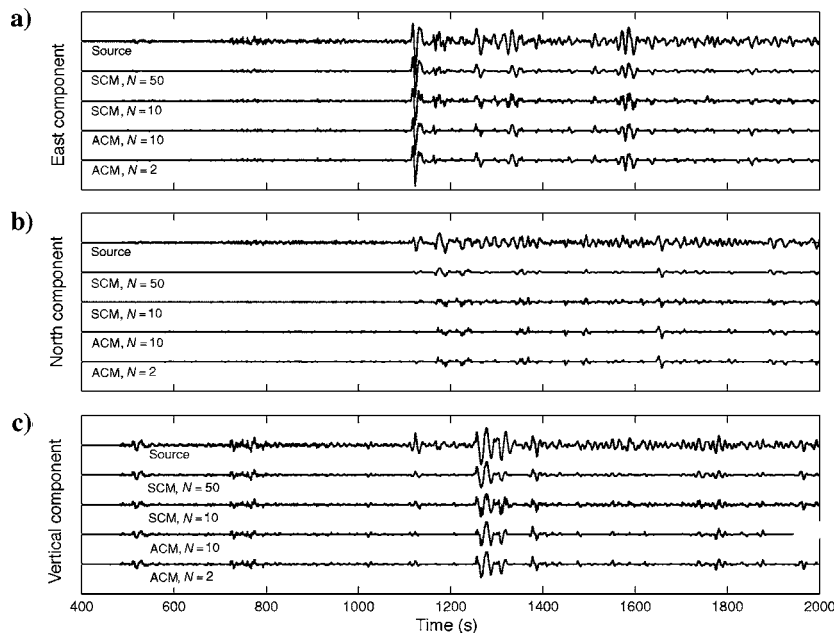


Figure 6. Comparison of filtering results with the covariance-based filter. (a) East component of the raw 3-C seismograms in Figure 4 with its filtered version using the SCM and the ACM; (b) and (c) show the north and vertical components. For the results from SCM, the window length T is given in several samples. For the seismograms obtained with the ACM, the window length is indirectly determined by the value N .

standard method, we note that for the small window (10 sample points), we observe high-frequency artifacts around the major events. These artifacts are greatly reduced as the size of the analysis window increases. The problem of finding the optimal window length to recover adequately the event of interest is the major limitation of the polarization filter associated with the SCM.

The ACM reduces the difference between the filtered seismograms around the arrival of the major events. Also, comparing major wave groups from filtered seismograms with the original, indicates that our method is less likely to create high-frequency artifacts. With

the ACM, increasing the window length (i.e., increasing N) mainly affects the sensitivity of the polarization analysis to a higher degree of polarization, but the method will not influence significantly the ratio of the first two eigenvalues that enter the polarization filter in equation 8. This explains why no major difference is observed between the filtered signals with $N = 2$ and $N = 10$. Overall, the filtering results from the two methods are comparable.

Our purpose with this example is to emphasize that with the ACM, the selection of the time window is not as critical as for the SCM. One can achieve a better performance of the polarization filter by using bandpass filtered signals with a zero-phase filter (Kanasewich, 1981).

CONCLUSIONS

We have introduced a method for estimating instantaneous-polarization attributes based on an approximation of the covariance matrix. The advantage of the proposed method over the standard method is that the length of the window size for the covariance computation is adjusted adaptively with the help of the instantaneous frequencies from the different components. Furthermore, because the polarization attributes are estimated for each time sample, no interpolation is needed. With the proposed method, one also can estimate the magnitude and direction of the third polarization direction in the case of a 3-C record. However, this estimate is not unique and is subject to the choice of the integer N that determines the size of the adaptive time window. The proposed method has potential application in wavefield separation and filtering of multicomponent seismic records using polarization analysis. For noise filtering of signals where seismic arrivals overlap, we think that the calculations in only the time domain or only in the frequency domain will not mitigate the noise as desired. In a forthcoming paper, an extension of the present method to the time-frequency domain using wavelet-transform techniques will be considered as a way to improve the polarization analysis for dispersive waves such as Rayleigh waves in heterogeneous media.

ACKNOWLEDGMENTS

This project is supported by a grant from the Deutsche Forschungsgemeinschaft (DFG) within the framework of the priority program SPP 1114, Mathematical Methods for Time-Series Analysis and Digital Image Processing. We thank Sergey Fomel, John Sumner, assistant editor Kees Wapenaar, editor Yonghe Sun, and the anonymous reviewers for constructive criticism that greatly improved the presentation of the manuscript.

REFERENCES

- Esmeroy, C., 1984, Polarization analysis, rotation and velocity estimation in three-component VSP, in M. N. Toksöz, and R. R. Stewart, eds. Vertical seismic profiling, part B: Advanced concepts: Geophysical Press, 236–255.
- Flinn, E. A., 1965, Signal analysis using rectilinearity and direction of particle motion: *Proceedings of the IEEE*, **59**, 1874–1876.
- Jackson, G. M., I. M. Mason, and S. A. Greenhalgh, 1991, Principal component transforms of triaxial recordings by singular value decomposition: *Geophysics*, **56**, 528–533.
- Jurkevics, A., 1988, Polarization analysis of three-component array data: *Bulletin of the Seismological Society of America*, **78**, 1725–1743.
- Kanasewich, E. R., 1981, *Time sequence analysis in geophysics*: University of Alberta Press.
- Montalbetti, J. R., and E. R. Kanasewich, 1970, Enhancement of teleseismic body phases with a polarization filter: *Geophysical Journal of the Royal Astronomical Society*, **21**, 119–129.
- Morozov, I. B., and S. B. Smithson, 1996, Instantaneous polarization attributes and directional filtering: *Geophysics*, **61**, 872–881.
- Reading, A. M., W. Mao, and D. Gubbins, 2001, Polarization filtering for automatic picking of seismic data and improved converted phase detection: *Geophysical Journal International*, **147**, 227–234.
- Soma, N., H. Niitsuma, and R. Baria, 2002, Reflection technique in time-frequency domain using multicomponent acoustic emission signals and application to geothermal reservoirs: *Geophysics*, **67**, 928–938.
- Vidale, J. E., 1986, Complex polarization analysis of particle motion: *Bulletin of the Seismological Society of America*, **76**, 1393–1405.